[^{68}Ga]Ga-RAYZ-8009: A Glypican-3–Targeted Diagnostic Radiopharmaceutical for Hepatocellular Carcinoma Molecular Imaging—A First-in-Human Case Series

Alex J. Poot[1,2], Constantin Lapa[3,4], Wolfgang A. Weber[4,5], Marnix G.E.H. Lam[1,2], Matthias Eiber[4,5], Alexander Dierks[3,4], Ralph A. Bundschuh[3,4], and Arthur J.A.T. Braat[1,2,6]

[1]Radiology and Nuclear Medicine, UMC Utrecht, Utrecht, The Netherlands; [2]Radiology and Nuclear Medicine, Princess Máxima Center, Utrecht, The Netherlands; [3]Nuclear Medicine, Faculty of Medicine, University of Augsburg, Augsburg, Germany; [4]Bavarian Cancer Research Center, Munich, Germany; [5]Department of Nuclear Medicine, School of Medicine and Health, TUM Klinikum, Technical University of Munich, Munich, Germany; and [6]Netherlands Cancer Institute, Amsterdam, The Netherlands

To date, the imaging and diagnosis of hepatocellular carcinoma (HCC) rely on CT/MRI, which have well-known limitations. Glypican-3 (GPC3) is a cell surface receptor highly expressed by HCC but not by normal or cirrhotic liver tissue. Here we report initial clinical results of GPC3-targeted PET imaging with [^{68}Ga]Ga-DOTA-RYZ-GPC3 (RAYZ-8009), a peptide-based GPC3 ligand in patients with known or suspected HCC. **Methods:** [^{68}Ga]Ga-RAYZ-8009 was obtained after labeling the peptide precursor with ^{68}Ga from a ^{68}Ge/^{68}Ga generator and heating at 90°C for 10 min followed by sterile filtration. After administration of [^{68}Ga]Ga-RAYZ-8009, a dynamic or static PET/CT scan was acquired between 45 min and 4 h after administration. Radiotracer uptake was measured by SUVs for the following tissues: suspected or actual HCC or hepatoblastoma lesions, non–tumor-bearing liver, renal cortex, blood pool in the left ventricle, and gastric fundus. Additionally, tumor–to–healthy-liver ratios (TLRs) were calculated. **Results:** Twenty-four patients (5 patients in the dynamic protocol; 19 patients in the static protocol) were scanned. No adverse events occurred. Two patients had no lesion detected and did not have HCC during follow-up. In total, 50 lesions were detected and analyzed. The mean SUV_{max} of these lesions was 19.6 (range, 2.7–95.3), and the mean SUV_{mean} was 10.1 (range, 1.0–49.2) at approximately 60 min after administration. Uptake in non–tumor-bearing liver and blood pool rapidly decreased over time and became negligible 45 min after administration (mean SUV_{mean}, <1.6), with a continuous decline to 4 h after administration (mean SUV_{mean}, 1.0). The opposite was observed for HCC lesions, for which SUVs and TLRs continuously increased for up to 4 h after administration. In individual lesion analysis, TLR was the highest between 60 and 120 min after administration. Uptake in the gastric fundus gradually increased for up to 45 min (to an SUV_{max} of 31.3) and decreased gradually afterward. **Conclusion:** [^{68}Ga]Ga-RAYZ-8009 is safe and allows for high-contrast imaging of GPC3-positive HCC, with rapid clearance from most normal organs. Thereby, [^{68}Ga]Ga-RAYZ-8009 is promising for HCC diagnosis and staging. Further research is warranted.

Key Words: hepatocellular carcinoma; HCC; GPC3; glypican-3; PET/CT

J Nucl Med 2024; 65:1597–1603
DOI: 10.2967/jnumed.124.268147

Hepatocellular carcinoma (HCC) is one of the leading causes of cancer-related death worldwide (*1*). Current guidelines (European Society for Medical Oncology, 2021; National Comprehensive Cancer Network, 2023) recommend CT and MRI for diagnosis of HCC (*2*). To structure reporting of CT and MRI for the primary lesion, the Liver Imaging Reporting and Data System (LI-RADS) classification has been widely adopted. LI-RADS was first released in 2011 and has since then undergone several updates (*3*). In LI-RADS, the likelihood of HCC is reported on a 5-point scale (LI-RADS 1 = definitively benign to LI-RADS 5 = definitively HCC) (*3*). However, the limitations of LI-RADS are also well established: at a high specificity (LI-RADS 5), the sensitivity is only 50%–70%. In LI-RADs 3 and 4, the frequency of HCC is neither low enough nor high enough to change patient management. Furthermore, no definitive positive diagnosis is feasible for subcentimeter lesions (*4*).

For extrahepatic disease, CT of the thorax and abdomen is considered to be sufficient, and additional skeletal scintigraphy for detection of bone metastases is not routinely advised. [^{18}F]FDG PET/CT has been investigated as an alternative for accurate disease staging; however, the metabolic activity of HCC is variable and [^{18}F]FDG PET/CT is therefore not generally suitable for HCC staging, although the degree of [^{18}F]FDG uptake correlates with tumor differentiation (*5,6*). To date, accurate HCC detection and staging with a molecular imaging modality are lacking.

Preclinical and histopathologic studies have sparked interest in glypican-3 (GPC3) for HCC. GPC3 is bound to the outer surface of the plasma membrane, overexpressed on HCC but barely detectable in normal tissues in adults (*7,8*). In histopathology studies using immunohistochemistry for GPC3, upregulation of GPC3 in HCC correlated with a poor prognosis (*9–11*). Because of the overexpression in HCC and the near absence of GPC3 expression in healthy tissue and cirrhotic liver, GPC3-targeted compounds have been an area of interest for several years (*12,13*). Recently, promising preclinical data on the potent selective GPC3-targeting peptide DOTA-RYZ-GPC3 (RAYZ-8009) were reported (*14*). On the basis of those promising results, we report the first-in-human results for RAYZ-8009 labeled with ^{68}Ga ([^{68}Ga]Ga-RAYZ-8009) from investigator-initiated clinical use imaging at 3 European institutions.

Received May 28, 2024; revision accepted Jul. 17, 2024.
For correspondence or reprints, contact Arthur J.A.T. Braat (a.j.a.t.braat@umcutrecht.nl).
Published online Sep. 12, 2024.

MATERIALS AND METHODS

Patient Population

We report on a retrospectively analyzed case series of patients with known or suspected primary or recurrent hepatocellular carcinoma (HCC) and pediatric patients with hepatoblastoma who underwent PET imaging with [^{68}Ga]Ga-RAYZ-8009 PET/CT because of unclear findings on conventional imaging studies. Because of the retrospective nature, the need for informed consent was waived by an Institutional Review Board. After administration, all patients were asked if they experienced any adverse events (e.g., nausea or pain). Patient demographics were collected and relevant medical history reported (e.g., underlying liver disease and Barcelona Criteria for Liver Cancer stage).

Radiopharmaceutical Preparation

The precursor peptide RAYZ-8009 for labeling was supplied by RayzeBio Inc. ^{68}Ga radiolabeling was performed using a clinically approved ^{68}Ge/^{68}Ga generator.

For [^{68}Ga]Ga-RAYZ-8009 production, 50 μg of RAYZ-8009 were dissolved in 200 μL of water for injection and pipetted into a mixing vial, to which 400 μL of ethanol and 800 μL of acetate buffer were added. The ^{68}Ge/^{68}Ga generator was eluted with 0.1 M HCl (6 mL). The concentrated ^{68}Ga was eluted with the 0.1 M HCl in a 5.0 M NaCl solution into the mixing vial containing the RAYZ-8009 solution. The mixture was heated to 90°C for 10 min and cooled to room temperature. The reaction mixture was diluted with 3 mL of 0.9% NaCl and passed through a 0.22-μM sterile filter into the product vial. After each production run, radionuclide purity was analyzed by half-time and γ-spectrum measurements. Radiochemical purity was analyzed by both instant thin-layer chromatography and high-performance liquid chromatography. pH was measured, and endotoxin content was determined. The sterility of each batch was ensured by sterility testing of a decayed sample of the product batch.

PET/CT Acquisition

For imaging acquisition, a 1–3 MBq/kg dose was administered, in line with other ^{68}Ga-labeled radiopharmaceuticals. Different imaging protocols were used. In the first 5 patients, dynamic PET/CT on a Siemens Biograph Vision V600 was performed. Simultaneously with injection of [^{68}Ga]Ga-RAYZ-8009, an image acquisition from the vertex to the thighs (with FlowMotion; Siemens) was initiated over 60 min (in frames of 4 × ~3.5 min, 3 × ~7.0 min, and 2 × ~15 min). In subsequent patients, static PET/CT was performed at a single (1 h) or multiple (40 min, 1 h, 2 h, 3 h, and 4 h) time points after administration over 7–15 min on a Biograph Vision (table speed, 1.6 mm/s; 4 iterations; 5 subsets; gaussian filter, 4 mm), a Siemens Biograph mCT (3 min/bed position; 4 iterations; 21 subsets; gaussian filter, 5 mm), or a GE HealthCare Discovery MI (2 min/bed position; 3 iterations; 21 subsets; gaussian filter, 5 mm). PET was reconstructed according to local practice. PET images were accompanied by a low-dose non–contrast-enhanced CT scan in 23 patients and by a diagnostic triple-phase CT scan in 1 patient. Prior contrast-enhanced CT or MRI was available for comparison in all patients.

PET/CT Interpretation

Qualitative interpretation was based on lesion detection by the local investigator. Qualitative assessments were compared with previous imaging studies (CT or MRI of the liver). In cases of underlying cirrhosis, chronic hepatitis B, or a previous history of HCC, the corresponding LI-RADS classification per lesion was obtained (*15*). Lesions not assessable according to LI-RADS were classified as "not assessable" (e.g., extrahepatic disease, hepatoblastoma origin, or noncirrhotic patients).

Semiquantitative assessment comprised body weight–corrected SUV_{max} and SUV_{mean} measurements, using volumes of interest and automated thresholding by 40% of the maximum pixel value within the volume of interest. Various compartments were analyzed, corresponding to tumors (HCC or hepatoblastoma), non–tumor-bearing liver (healthy-liver activity [HL]; at least 3 cm^3), renal cortex, blood-pool activity in the left ventricle (at least 1 cm^3 volume of interest), and gastric fundus. Additionally, the following tumor–to–healthy-liver ratios (TLRs) were calculated: mean TLR (TLR_{mean}) (HCC SUV_{mean} divided by HL SUV_{mean}) and maximum TLR (TLR_{max}) (HCC SUV_{max} divided by HL SUV_{max}) as measures of target-to-background ratios. Tumor–to–blood-pool ratios (TBPRs) were calculated in the same fashion and reported.

Statistical Analysis

Baseline characteristics of the patients were summarized using descriptive statistics. Qualitative imaging assessment was binary (lesion was visible or not) and reported. Semiquantitative assessment included descriptive statistics and in-patient comparison between HL and tumor uptake. Furthermore, to visually illustrate the dynamic data and later-time-point results (i.e., biodistribution), all measurements were combined and a mean SUV_{mean} graph was plotted for all different compartments. For all separate lesions, if applicable, a LI-RADS classification was reported. When LI-RADS classification was not applicable (i.e., lesions were classified as not assessable), these lesions were combined as a separate group, for completeness of data representation. Differences in [^{68}Ga]Ga-RAYZ-8009 uptake per LI-RADS category and "not applicable" group were tested using a Kruskal–Wallis H test. Differences in [^{68}Ga]Ga-RAYZ-8009 uptake per lesion size (grouped data: 0–3, 3–5, 5–10 and > 10 cm) were tested using a Kruskal–Wallis H test.

RESULTS

Patient Population

Twenty-four patients were scanned (22 adults with suspected or actual HCC and 2 children with hepatoblastoma), of whom 5 underwent the dynamic protocol (all adults) and 19 a static scan (12 single- and 7 multiple-time-point static). One adult suspected to have HCC and 1 child suspected to have recurrent hepatoblastoma recurrence had a negative PET/CT scan. During clinical and imaging follow-up (3–9 mo), both did not develop malignant hepatic disease (recurrence). These 2 cases were included for healthy-tissue semiquantitative measurements. Of the remaining 22 cases, all 21 adults had at least 1 HCC (3 patients had 1 and 2 patients had 2 extrahepatic metastases of HCC) and 1 child had a lymph node recurrence of a previously treated hepatoblastoma.

In total, 50 lesions were included: 7 LI-RADS 3, 13 LI-RADS 4, 17 LI-RADS 5, and 13 nonassessable lesions. Baseline characteristics are presented in Table 1.

Radiochemistry

The production of [^{68}Ga]Ga-RAYZ-8009 was automated and proved to be highly reliable. Near-quantitative radiolabeling yields were obtained, though total quantities of product were dependent on the generator used. The robustness of the procedure was demonstrated in the 3 consecutive validation runs for [^{68}Ga]Ga-RAYZ-8009 followed by 18 repetitive production runs, all with good yields and purity (Table 2). [^{68}Ga]Ga-RAYZ-8009 is highly stable, as was demonstrated by radio–high-performance liquid chromatography analysis at 3 h after production. In all validation runs, less than 1% product radiolysis was observed.

The mean ± SD of the administered mass of [^{68}Ga]Ga-RAYZ-8009 was 18 ± 7 μg (range, 10–27 μg). The mean administered activity was 150 MBq (range, 74–221 MBq). There were no adverse or clinically detectable pharmacologic effects in any of the 24 subjects.

TABLE 1
Baseline Characteristics

Characteristic	Data
Age (y)	67 (12–85)
HCC size (mm)	32 (3–131)
[^{68}Ga]Ga-RAYZ-8009 activity administered (MBq)	150 (74–221)
Underlying liver disease*	
Alcohol-associated liver disease	9 (37%)
Metabolic dysfunction–associated steatotic liver disease	5 (21%)
Hepatitis B	3 (13%)
Hepatitis C	1 (4%)
Hemochromatosis	1 (4%)
No underlying disease	5 (21%)
Child–Pugh score	
A	19 (79%)
B	4 (17%)
C	1 (4%)
Barcelona criteria for liver cancer	
A	3 (13%)
B	7 (29%)
C	11 (45%)
Not applicable	3 (13%)
Portal vein tumor thrombus	
Yes	3 (13%)
No	21 (87%)
Disease extension	
Unifocal disease	12 (50%)
Multifocal disease	12 (50%)
Extrahepatic disease	
Yes	4 (17%)
No	20 (83%)
Prior treatment	
No	15 (63%)
Radioembolization	5 (21%)
Radioembolization, chemoembolization, atezolizumab + bevacizumab	1 (4%)
Ablation	1 (4%)
Gemcitabine + cisplatin	1 (4%)
Cisplatin + doxorubicin + liver transplantation	1 (4%)

*Adhering to new international nomenclature (*25*).
Qualitative data are number and percentage; continuous data are mean and range.

TABLE 2
Production and Quality Control Results of [^{68}Ga]Ga-RAYZ-8009

Quality control test	Specification	Production results (n = 18)
Appearance	Clear/colorless	Yes
Radiochemical purity (radio–high-performance liquid chromatography)	>95%	99.23 ± 0.78
Radiochemical purity		
Instant thin-layer chromatography eluent A	>97%	98.46 ± 0.51
Instant thin-layer chromatography eluent B	>97%	99.55 ± 0.29
pH	3.5–5	4.27 ± 0.06

Dynamic Scanning

In 5 patients, dynamic PET was performed. After administration of a 2 MBq/kg dose of [^{68}Ga]Ga-RyZ-GPC3, the in vivo biodistribution and renal clearance could be observed within minutes (Fig. 1). HCC lesions could already be visualized in the first acquisition, because of the hypervascular nature of the tumor (Fig. 1). Static images at 60 min after administration (range, 51–75 min after administration) resulted in a high image quality visually (Fig. 1), with the highest TLR and TBPR in the dynamic dataset (median TLR_{max}, 4.3; median TLR_{mean}, 4.6; median maximum TBPR ($TBPR_{max}$), 4.0; and median mean TBPR ($TBPR_{mean}$), 3.5; 19 lesions).

Semiquantitative measurements of the dynamic PET/CT data are presented in Figure 2 and showed a rapid decrease in HL and blood-pool activity in the left ventricle, becoming negligible approximately 30 min after administration (mean SUV_{mean}, <1.5). Kidney accumulation fluctuated over time, whereas gastric wall accumulation steadily increased in the first 45 min and gradually declined thereafter (Fig. 2).

Static Imaging

In the entire dataset including 50 lesions, at around 1 h after administration (range, 44–75 min), median TLR_{max} was 8.5 (range, 0.9–47.7) and median TLR_{mean} was 7.5 (range, 0.8–41). When patients in only the slot at 1 h after administration were considered (range, 51–75 min), 39 lesions could be included, with a mean TLR_{max} of 8.3 (range, 0.9–47.7) and a mean TLR_{mean} of 7.5 (range, 0.8–41). In 6 patients with an acquisition at 2 h after administration (range, 120–136 min), including 8 lesions, median TLR_{max} and median TLR_{mean} were 7.7 and 7.2, respectively. In 5 patients with an acquisition at 4 h after administration (range, 235–252 min), including 7 lesions, median TLR_{max} and median TLR_{mean} were 8.8 and 10.0, respectively (Table 3).

Disease Heterogeneity

In total, 50 tumors (43 primary HCCs, 1 lung metastasis, 1 soft-tissue metastasis, 3 lymph node metastases, 1 bone metastasis, and 1 hepatoblastoma lymph node metastasis) were analyzed. In 4 patients, GPC3 uptake was clearly heterogeneous, either being treatment-naïve (n = 2) or having received local or systemic therapy before (n = 2). Even within a single patient, clear differences in GPC3 expression were encountered (Fig. 3). Of all measured lesions (n = 50), TLR_{max} was at least 2 in 40 of 50 (80%), at least 3 in 35 of 50 (70%), and at least 5 in 23 of 50 (46%), and for TLR_{mean} the respective values were 35 of 50 (70%), 32 of 50 (64%), and 26 of 50 (52%). All but 1

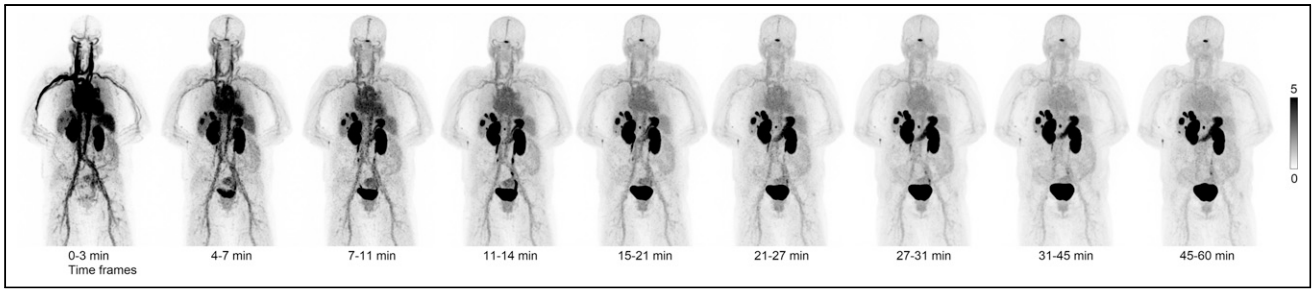

FIGURE 1. Dynamic PET/CT images of woman with multifocal bilobar HCC.

lesion had a TLR_{max} or TLR higher than 1.0. For TBPR, in all measured lesions $TBPR_{max}$ was at least 2 in 45 of 50 (90%), at least 3 in 39 of 50 (78%), and at least 5 in 29 of 50 (58%), and for $TBPR_{mean}$ the respective values were 38 of 50 (76%), 30 of 50 (60%), and 22 of 50 (44%). All lesions had a $TBPR_{max}$ and $TBPR_{mean}$ higher than 1.0 (Table 3).

In this limited number of extrahepatic disease cases, no distinct difference in [^{68}Ga]Ga-RAYZ-8009 uptake was noticed from primary HCCs in qualitative assessments (Fig. 4). Three patients had a portal vein tumor thrombus, and all 3 thrombi were GPC3-positive on qualitative assessment. Two patients had other concurrent malignancies: one patient had concurrent adenocarcinoma of the prostate with regional lymph node metastases (Fig. 3; GPC3-negative), and another had concurrent metastatic breast carcinoma (lymph nodes and diffuse bone metastases; all GPC3-negative qualitatively) and bladder carcinoma (local disease only; GPC3-negative qualitatively). In the latter patient, diffuse sclerotic bone lesions on CT were reported as part of her breast carcinoma, but after the [^{68}Ga]Ga-RAYZ-8009 PET/CT acquisition, 1 distinct lesion had intense uptake and was biopsy-proven to be metastasis of her HCC.

GPC3 Accumulation Versus LI-RADS and Size

A wide variety of primary HCC sizes was included, with a mean longest diameter of 32 mm (range, 3–131 mm). Primary HCCs were also analyzed according to their LI-RADS classification, and no significant difference was found between the different categories and [^{68}Ga]Ga-RAYZ-8009 uptake (Fig. 4). No significant difference

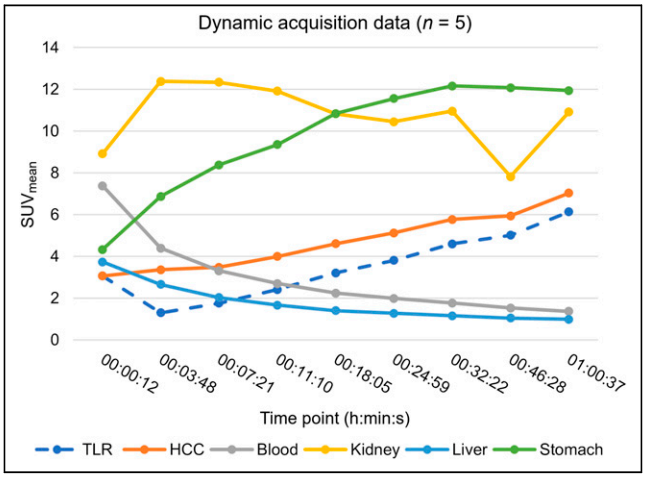

FIGURE 2. Data of 5 patients with dynamic imaging. All lines are SUV_{mean}, except for TLR, which depicts mean TLR_{mean}.

was found between [^{68}Ga]Ga-RAYZ-8009 uptake and lesion size ($P > 0.3$; Supplemental Fig. 1; supplemental materials are available at http://jnm.snmjournals.org).

DISCUSSION

This initial clinical evaluation of GPC3 imaging with a novel peptide ligand showed rapid and intense accumulation of [^{68}Ga]Ga-RAYZ-8009 in HCC and hepatoblastoma, whereas uptake in normal or cirrhotic liver was low. This resulted in an average tumor-to-liver uptake ratio of more than 7.5 at 60 min after administration. [^{68}Ga]Ga-RAYZ-8009 rapidly cleared from the bloodstream, and only the kidney and the stomach demonstrated significant retention of the radiotracer. No clinical side effects of [^{68}Ga]Ga-RAYZ-8009 were observed. The radiolabeling of [^{68}Ga]Ga-RAYZ-8009 proved to be straightforward with close to 100% radiochemical yields, making the production of this PET tracer highly reliable.

GPC3 is a member of the glypican family of proteoglycans, defined as proteins with extensive glycosylation by heparan sulfate glycosaminoglycans. GPC3 is bound to the outer surface of the plasma membrane by a glycosylphosphatidylinositol anchor and can stimulate or inhibit the interaction of various growth factors (e.g., Wnt and hedgehog) with their cognate receptors (*16–19*). GPC3 is highly expressed in the placenta and embryonic tissues, where it plays a critical role in the morphogenesis of various organs (*16,20*). In contrast, GPC3 expression in postnatal tissue is highly restricted, with no detectable RNA in most organs and very low expression levels in the lungs and kidneys (*20*). However, GPC3 expression is commonly reactivated in HCCs and hepatoblastomas. Approximately 70% of HCCs markedly overexpress GPC3 at the RNA or protein level (*20,21*). The degree of GPC3 expression is an adverse prognostic factor in HCC. Shirakawa et al. reported their results in 107 surgical specimens, after hepatectomy for an HCC (*10*). In their cohort, GPC3 expression correlated with disease aggressiveness; GPC3-negative tumors (<10% positive cells at immunohistochemistry) more often were well-differentiated tumors, whereas GPC3-positive tumors (>10% positive cells at immunohistochemistry) were more often moderately or poorly differentiated tumors. This was reflected in their clinical follow-up; GPC3-positive patients showed a significantly lower 5-y survival rate (54.5%) than patients with a GPC3-negative HCC (87.7%; $P = 0.031$). Furthermore, no disease-related deaths were observed in the 20 GPC3-negative cases during a median follow-up of 3.7 ± 2.1 y, compared with a 3-y survival rate of 62.5% in the GPC3-positive cases. Similar correlations were described by Kaseb et al. in their retrospective cohort of 101 patients (*9*). Specifically in the cohort primarily treated with surgical resection ($n = 56$), GPC3-positive disease correlated with a worse overall survival

TABLE 3
Semiquantitative Measures of Tumors and Physiologic Uptake at Different Time Points

Measure	1 h after injection	2 h after injection	4 h after injection
Lesions	39	8	7
Patients	18	6	5
SUV_{max}	11.8 (2.7–95.3)	29.7 (9.9–137.9)	28.9 (12–124.3)
SUV_{mean}	6.4 (1.0–49.2)	17.7 (5.1–60.8)	15.4 (6.8–74)
TLR_{max}	5.0 (0.9–47.7)	7.7 (3.8–60.3)	8.8 (3.8–4.9)
TLR_{mean}	5.1 (0.8–41)	7.2 (2.7–60.8)	10.0 (41.4–56.9)
$TBPR_{max}$	4.0 (1.6–15.3)	5.5 (1.5–56.1)	10.3 (4.0–89.7)
$TBPR_{mean}$	3.3 (1.0–16.2)	4.7 (1.0–29.4)	7.2 (3.2–52.6)
SUV_{mean}, blood pool	1.6 (0.9–2.4)	1.4 (1.1–1.6)	1.0 (0.7–1.4)
SUV_{mean}, liver	1.3 (0.7–2.4)	1.7 (1.0–2.3)	1.7 (1.3–2.5)
SUV_{mean}, kidney	12.5 (6.4–17.5)	16.7 (9.4–19.7)	21.2 (11.6–25.2)
SUV_{mean}, gastric fundus	10.2 (1.8–21.9)	13.4 (4.8–18.2)	10.1 (2.2–13.3)

Qualitative data are number; continuous data are median and range.

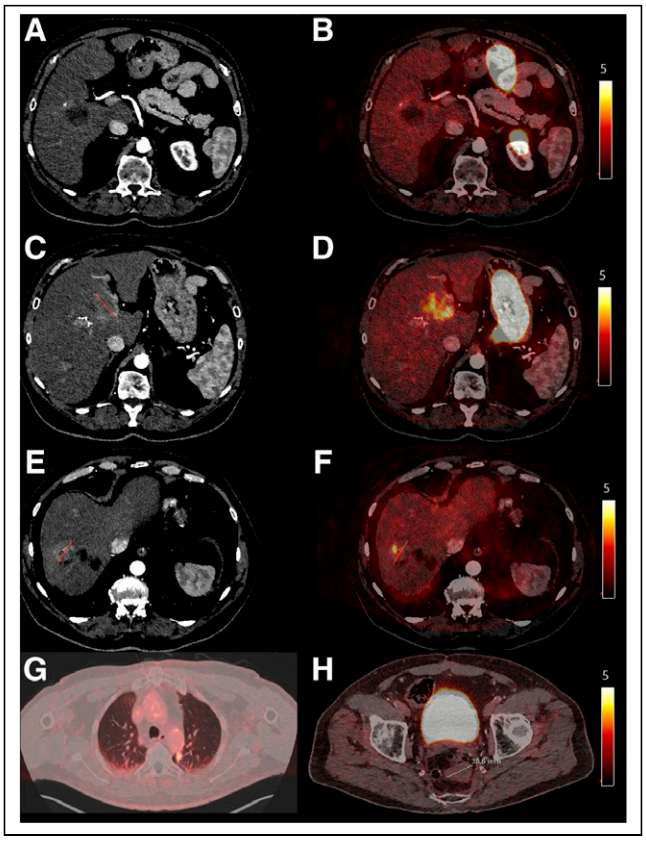

FIGURE 3. Disease with GPC3 heterogeneity in 66-y-old patient with biopsy-proven GPC3-negative HCC in segment 5/6 (A and B), clear GPC3-positive tumor in segment 8 (C and D), heterogeneous HCC in segment 7 with only focal accumulation on [^{68}Ga]Ga-RAYZ-8009 PET (E and F), GPC3-positive lung metastasis in posterior of aortic arch in left upper lobe (G), and biopsy-proven GPC3-negative adenocarcinoma of prostate with lymph node metastases (H). Arrows indicate the findings. (A, C, and E) Contrast-enhanced CT imaging. (B, D, F, and G) [^{68}Ga]Ga-RAYZ-8009 PET overlay. (H) [^{68}Ga]Ga-RAYZ-8009 PET/CT with nonenhanced low-dose CT.

(median overall survival, 36 vs. 159 mo). These reported findings are in line with other available literature on GPC3 expression (*11*).

Previous studies have investigated the use of antibodies targeting GPC3 by radiolabeling with either ^{124}I or ^{89}Zr. In a phase 1 study with codrituzumab (ClinicalTrials.gov identifier NCT00976170), a substudy with [^{124}I]I-codrituzumab PET/CT was performed (*12*). PET/CT was performed within 1–4 h of infusion and 1, 2–3, and 4–6 d after administration. The authors reported the maximum accumulation of the radiolabeled antibody at 24 h after administration, after which the accumulation declined. In line with other iodine-labeled pharmaceuticals, thyroid accumulation increased over time, whereas other sites showed a gradual decrease of accumulation. Seven of 14 patients (50%) had a TBPR of more than 2, and 11 of

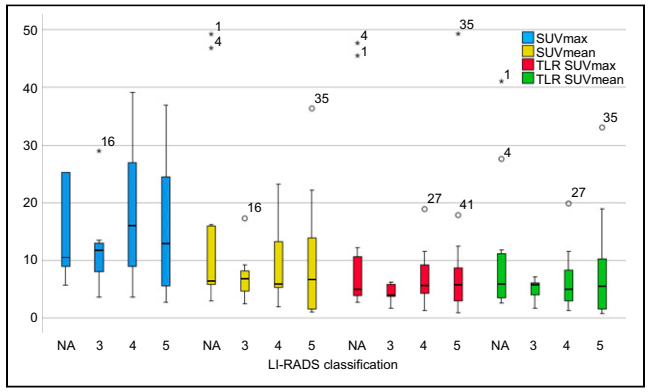

FIGURE 4. Box plot per [^{68}Ga]Ga-RAYZ-8009 measurements at 1-h time point (absolute values on *y*-axis) and LI-RADS classification (*x*-axis). No significant difference was observed between different LI-RADS classifications and [^{68}Ga]Ga-RAYZ-8009 measurements (*P* values: SUV_{max}, 0.78; SUV_{mean}, 0.66; TLR SUV_{max}, 0.67; and TLR SUV_{mean}, 0.75), as depicted in absolute values (SUV_{max} and SUV_{mean}) and TLR SUV_{max} and TLR SUV_{mean}. NA = not applicable (extrahepatic metastases or hepatoblastoma lesion) or not available (in absence of multiphase contrast-enhanced cross-sectional imaging).

14 (79%) had a TBPR of more than 1. Even though difficult to compare (peptide vs. antibody), these results seem similar to the current study with [^{68}Ga]Ga-RAYZ-8009 ($TBPR_{mean}$, >2 in 76%); however, a TBPR of more than 1 was seen in all patients, including in biopsied lesions with GPC3-negative immunohistochemistry (Fig. 2).

The distribution of [^{68}Ga]Ga-RAYZ-8009 in the current study in patients resembled the distribution found in mice (*14*). In our study, [^{68}Ga]Ga-RAYZ-8009 also showed an accumulation in the stomach wall that peaked at around 30 min after administration and slowly declined thereafter (Fig. 2). To our knowledge, GPC3 expression in the stomach is minimal (*22,23*). This suggests that stomach uptake of [^{68}Ga]Ga-RAYZ-8009 is not mediated by GPC3 binding. The different kinetics of radiotracer uptake over time by the stomach and HCC lesions also point in this direction. Future studies are required to clarify the uptake mechanism of [^{68}Ga]Ga-RAYZ-8009 in the stomach.

Low uptake of [^{68}Ga]Ga-RAYZ-8009 in some HCCs was expected because about 30% of HCCs do not express GPC3 (*20,21*). If confirmed by larger studies, [^{68}Ga]Ga-RAYZ-8009 could therefore provide important complementary information to the LI-RADS classification by CT and MRI. According to a systematic review, the frequency of HCC in the different LI-RADS categories is as follows: 0% HCC in LI-RADS 1, 13% HCC in LI-RADS 2, 38% HCC in LI-RADS 3, 74% HCC in LI-RADS 4, and 94% HCC in LI-RADS 5 (*24*). Especially in LI-RADS 3 and 4, GPC3 uptake may impact patient management by significantly increasing the overall likelihood of HCC diagnosis. The potential additional diagnostic information of [^{68}Ga]Ga-RAYZ-8009 PET is supported by our observation that high tracer uptake was observed in HCCs, irrespective of LI-RADS score (Fig. 4). The findings of this initial clinical study may provide guidance on the areas of future studies with [^{68}Ga]Ga-RAYZ-8009.

This initial report of the diagnostic performance of [^{68}Ga]Ga-RAYZ-8009 has limitations: First, the patient population was relatively small and was heterogeneous, and the clinical indication for the scan was highly variable. Furthermore, PET/CT scanner types and acquisition and reconstruction protocols differed between the centers. Finally, not all HCC lesions were histologically verified or confirmed with standardized imaging follow-up, which may have caused an overestimation of the specificity of [^{68}Ga]Ga-RAYZ-8009 PET/CT imaging for detection of HCC or hepatoblastoma. The impact of [^{68}Ga]Ga-RAYZ-8009 PET/CT findings on clinical patient management is outside the scope of this work. Therefore, further research is warranted to confirm [^{68}Ga]Ga-RAYZ-8009 PET/CT imaging findings with histopathology and their utility in future clinical practice in larger or better-defined populations. With the favorable distribution seen in this case series, radiolabeling of RAYZ-8009 with a β- or α-emitting isotope may have potential as a therapeutic radiopharmaceutical in the near future.

CONCLUSION

[^{68}Ga]Ga-RAYZ-8009 is a peptide-based PET tracer that is safe and allows for high-contrast molecular imaging of HCC in humans, with a rapid and favorable biodistribution. Future studies are warranted to assess the potential of [^{68}Ga]Ga-RAYZ-8009 to improve diagnosis and staging of HCC.

DISCLOSURE

Constantin Lapa reports prior consulting activities for Blue Earth Diagnostics Ltd., PentixaPharm, Pfizer, and Novartis. Wolfgang Weber is on advisory boards and receives compensation from Blue Earth Diagnostics, ITM, and PentixaPharm. He has received research support from Blue Earth Diagnostics, Novartis, Roche Diagnostics, and Siemens Healthineers. Marnix Lam is consultant for Boston Scientific and Terumo and receives research support from Boston Scientific, Terumo, and Novartis. Matthias Eiber owns stocks or has other ownership interests in Novartis and Telix Pharmaceuticals; has a consultancy or advisory role with Blue Earth Diagnostics, ABX Advanced Biochemical Compounds, Janssen Oncology, Telix Pharmaceuticals, and Novartis; receives research funding from Siemens, ABX Advanced Biochemical Compounds, Blue Earth Diagnostics, and Bayer; has a patent application for rhPSMA; and receives travel funds from Bayer Schering Pharma. Ralph Bundschuh receives honoraria from Eisai AG and has a consultancy or advisory role with Bayer. Arthur Braat is a consultant for Boston Scientific, Terumo, and GE HealthCare and receives research support from Ariceum Therapeutics. This research was financially supported by RayzeBio, Inc., and the precursor was provided by RayzeBio, Inc. No other potential conflict of interest relevant to this article was reported.

KEY POINTS

QUESTION: What are the imaging characteristics with [^{68}Ga]Ga-RAYZ-8009 in patients?

PERTINENT FINDINGS: GPC3-targeted molecular imaging with [^{68}Ga]Ga-RAYZ-8009 PET/CT showed a rapid and favorable in vivo biodistribution, with high tumor accumulation in HCC and hepatoblastoma and a near absence of accumulation in normal and cirrhotic liver, as well as in most normal organs.

IMPLICATIONS FOR PATIENT CARE: The fast and favorable biodistribution of [^{68}Ga]Ga-RAYZ-8009 is indicative of high clinical potential for disease detection and staging in HCC and hepatoblastoma.

REFERENCES

1. Sung H, Ferlay J, Siegel RL, et al. Global cancer statistics 2020: GLOBOCAN estimates of incidence and mortality worldwide for 36 cancers in 185 countries. *CA Cancer J Clin.* 2021;71:209–249.
2. Vogel A, Cervantes A, Chau I, et al. Hepatocellular carcinoma: ESMO clinical practice guidelines for diagnosis, treatment and follow-up. *Ann Oncol.* 2018;29: iv238–iv255.
3. Chernyak V, Fowler KJ, Kamaya A, et al. Liver imaging reporting and data system (LI-RADS) version 2018: imaging of hepatocellular carcinoma in at-risk patients. *Radiology.* 2018;289:816–830.
4. Chernyak V, Fowler KJ, Do RKG, et al. LI-RADS: looking back, looking forward. *Radiology.* 2023;307:e222801.
5. Boussouar S, Itti E, Lin SJ, et al. Functional imaging of hepatocellular carcinoma using diffusion-weighted MRI and ^{18}F-FDG PET/CT in patients on waiting-list for liver transplantation. *Cancer Imaging.* 2016;16:4.
6. Hyun SH, Eo JS, Song BI, et al. Preoperative prediction of microvascular invasion of hepatocellular carcinoma using ^{18}F-FDG PET/CT: a multicenter retrospective cohort study. *Eur J Nucl Med Mol Imaging.* 2018;45:720–726.
7. Filmus J, Capurro M, Rast J. Glypicans. *Genome Biol.* 2008;9:224.
8. Haruyama Y, Kataoka H. Glypican-3 is a prognostic factor and an immunotherapeutic target in hepatocellular carcinoma. *World J Gastroenterol.* 2016;22: 275–283.
9. Kaseb AO, Hassan M, Lacin S, et al. Evaluating clinical and prognostic implications of Glypican-3 in hepatocellular carcinoma. *Oncotarget.* 2016;7:69916–69926.
10. Shirakawa H, Suzuki H, Shimomura M, et al. Glypican-3 expression is correlated with poor prognosis in hepatocellular carcinoma. *Cancer Sci.* 2009;100:1403–1407.

11. Jiang D, Zhang Y, Wang Y, Xu F, Liang J, Wang W. Diagnostic accuracy and prognostic significance of Glypican-3 in hepatocellular carcinoma: a systematic review and meta-analysis. *Front Oncol.* 2022;12:1012418.
12. Carrasquillo JA, O'Donoghue JA, Beylergil V, et al. I-124 codrituzumab imaging and biodistribution in patients with hepatocellular carcinoma. *EJNMMI Res.* 2018;8:20.
13. Fayn S, King AP, Gutsche NT, et al. Site-specifically conjugated single-domain antibody successfully identifies glypican-3-expressing liver cancer by immuno-PET. *J Nucl Med.* 2023;64:1017–1023.
14. Lin F, Clift R, Ehara T, et al. Peptide binder to glypican-3 as a theranostic agent for hepatocellular carcinoma. *J Nucl Med.* 2024;65:586–592.
15. Terzi E, Ayuso C, Piscaglia F, Bruix J. Liver imaging reporting and data system: review of pros and cons. *Semin Liver Dis.* 2022;42:104–111.
16. Filmus J. The function of glypicans in the mammalian embryo. *Am J Physiol Cell Physiol.* 2022;322:C694–C698.
17. Fernández D, Guereno M, Lago Huvelle MA, Cercato M, Peters MG. Signaling network involved in the GPC3-induced inhibition of breast cancer progression: role of canonical Wnt pathway. *J Cancer Res Clin Oncol.* 2018;144:2399–2418.
18. Liu YC, Wierbowski BM, Salic A. Hedgehog pathway modulation by glypican 3-conjugated heparan sulfate. *J Cell Sci.* 2022;135:jcs259297.
19. Grega SD, Zheng DX, Zheng QH. Imaging ligands targeting glypican-3 receptor expression in hepatocellular carcinoma. *Am J Nucl Med Mol Imaging.* 2022;12:113–121.
20. Hsu HC, Cheng W, Lai PL. Cloning and expression of a developmentally regulated transcript MXR7 in hepatocellular carcinoma: biological significance and temporospatial distribution. *Cancer Res.* 1997;57:5179–5184.
21. Capurro M, Wanless IR, Sherman M, et al. Glypican-3: a novel serum and histochemical marker for hepatocellular carcinoma. *Gastroenterology.* 2003;125:89–97.
22. GPC2. GEPIA website. http://gepia.cancer-pku.cn/detail.php?gene=GPC3. Accessed August 26, 2024.
23. GPC3. The Human Protein Atlas website. https://www.proteinatlas.org/ENSG00000147257-GPC3/summary/rna. Accessed August 26, 2024.
24. van der Pol CB, Lim CS, Sirlin CB, et al. Accuracy of the liver imaging reporting and data system in computed tomography and magnetic resonance image analysis of hepatocellular carcinoma or overall malignancy: a systematic review. *Gastroenterology.* 2019;156:976–986.
25. Rinella ME, Lazarus JV, Ratziu V, et al. A multisociety Delphi consensus statement on new fatty liver disease nomenclature. *Hepatology.* 2023;78:1966–1986.